Customized Handling of Unintended Interface Operation in Assistive Robots

Deepak Gopinath*[1,3], Mahdieh Nejati Javaremi*[1,3] and Brenna Argall[1,2,3]

***Abstract*— We present an assistance system that reasons about a human's *intended* actions during robot teleoperation in order to provide appropriate modifications on unintended behavior. Existing methods typically treat the human and control interface as a black box and assume the measured user input is noise-free, and use this signal to infer task-level human intent. We recognize that the signal measured through the interface is masked by the physical limitations of the user and the interface they are required to use. With this key insight, we model the human's physical interaction with a control interface during robot teleoperation, and distinguish between interface-level *intended* and *measured* physical actions explicitly. By reasoning over the unobserved intentions using model-based inference techniques, our assistive system provides customized modifications on a user's issued commands. We validate our algorithm both in simulation and with a 10-person human subject study in which we evaluate the performance of the proposed assistance paradigms. Our results show that the assistance paradigms helped to significantly reduce task completion time, number of mode switches, cognitive workload, and user frustration, and improve overall user satisfaction.**

I. INTRODUCTION

One of the most promising application domains for shared human-robot control is assistive devices. In this domain, robotics autonomy collaborates with a human in the operation of their assistive device, with the aim of increasing that human's independence and safety. In addition to its utility as a control signal, the human's input often is used in various other capacities by the robotics autonomy, such as input to an inference engine. Deviations—in magnitude, direction, or timing—between the true signal intended by the human and that received by the autonomy thus can have rippling effects throughout the control system. Critically, within this domain, the *source* of the human's signal overwhelmingly is treated as a black box. However, not only might the human's issued signal be dramatically impacted by their motor impairment, limitations of the interface accessible to them to operate the assistive device often mask their true signal intent. We posit that to consider the source of the human control signal, and its influence on the correctness of the signal issued, is critical.

When a person is fit for a powered wheelchair, arguably the most ubiquitous powered assistive device, the seating clinician will choose the control interface based on the user's unique physical abilities and constraints. Operating a control interface requires the human to *physically activate* the interface—whether via button press, joystick deflection [1], screen tap [2], or even electrical signals issued by muscles [3] or by the brain [4]. The signal which results then is mapped to the control space of the device. Neither this activation, nor this mapping, typically is represented within a robotics autonomy system. Instead, the robot control signal which results is represented in isolation—independent of the activation or mapping mechanisms. However, prior work has shown the type of control interface to significantly effect the timing, transient noise, and accuracy of a signal issued to operate an assistive device [5]. Moreover, when used in partnership with robotics autonomy, when the autonomy is *not* aware of such interface usage characteristics as the activation and mapping mechanisms, the overall performance of the shared-control system degrades [5]. The suggestion is of a need for explicit modeling of the user's physical interaction with the interface, and that *interface-awareness* is a key component to the design of successful assistive shared-autonomy algorithms.

In this work, we introduce a mathematical model that formalizes the human's physical interaction with the interface and then use this model to provide customized adjustments on their issued commands within a shared-control framework. Specifically, our contributions are threefold:

a) Modeling the User's Physical Interface Operation: We mathematically formulate the user's *physical interaction* with the control interface during teleoperation—specifically, how intended user inputs are altered through the interface before being measured by the system. We use data collected from the person to build *user-specific* models of control mapping and stochastic deviations from intended commands to *personalize* the modulating assistive algorithms.

b) Model-Based Inference of Intended Input: Using the interface-aware physical interaction model and prior knowledge of the user's high-level behavior, we employ probabilistic reasoning over latent intended user control commands to deduce unintended deviations from optimal behavior. Notably, the strength of our method is that it does not require any additional sensor streams for improving prediction accuracy.

c) Customized Corrective Assistance: We formulate two methods to provide appropriate modifications to the measured human control input in an *online* fashion. The assistance algorithm is personalized to the user because the user-specific probabilistic models encode the idiosyncrasies of a particular user's interaction behavior with the robot.

*Equal contribution

[1]Department of Mechanical Engineering, Northwestern University, Evanston, IL, USA

[2]Department of Computer Science, Northwestern University, Evanston, IL, USA

[3]Shirley Ryan AbilityLab, Chicago, IL, USA

II. RELATED WORK

User Input Noise. Deviations between intended and produced human motions have been extensively studied [6], [7], [8] and can arise due to cognitive as well as physiological factors [9]. For motor-impaired people, inherent physical limitations can increase the likelihood of accidental deviations from intended commands, which can lead to unwanted robot behavior. Therefore, in a shared-autonomy system it is important for the autonomy to make decisions based on *intended*, as opposed to measured and executed, interface actions to improve the quality of the interaction: thus, the need for command-level intent inference.

Command-level Inference. Most research aimed at advancing teleoperation systems has focused on creating novel devices that improve upon various aspects of the teleoperation system, such as improved signal decoding in a brain machine interface [10], haptic feedback for increased transparency [11], or improved fixed mappings from user inputs to control commands in a redundant body machine interface [12]. Little work in assistive robotics has distinguished between the intended versus produced command signal measured through the interface. Work in driver behavior modeling has investigated higher-level (action-level) inference, for example, to classify and predict driver actions [13]. Another work considers the uncertainty in human grasp intent to provide appropriate autonomous robotic grasp plans [14]. Unlike our work, they assume the human is physically capable of producing intended commands and the source of uncertainty is due to detection noise. Previous work has modeled a person's internal beliefs about a dynamic system, and uses an internal-to-true dynamics transfer function in order to provide the assistance that leads to a desired human action or learning outcome [15], [16]. In these works it is assumed that any suboptimal human command is due to a mismatch between their internalized and the true dynamics model, plus there is no control sharing—the autonomy alone is issuing commands based on the inferred user intent.

Intent Inference for Shared Control. Shared-control assistive systems often require a good estimate of the user's intent—which could be a high-level goal such as a navigation landmark to drive a wheelchair towards or an object to grasp using an assistive robotic arm [17]. Bayesian inference based approaches are widely used in the context of shared control in which the user is modelled as a Markov Decision Process and is assumed to be noisily optimizing some cost function with respect to a high-level goal [18], [19]. In this work we take a more fine-grained approach to modeling teleoperation, in which we explicitly distinguish the intended and measured interface-level physical actions.

III. MOTIVATION: INTERFACE-AWARE SIGNAL INTERPRETATION

We postulate that modeling how physical actions are mapped to task-level actions and how the control signal is then altered through the interface will help the autonomy to *reason about deficiencies* in human teleoperation in order to *improve the quality* of robot teleoperation.

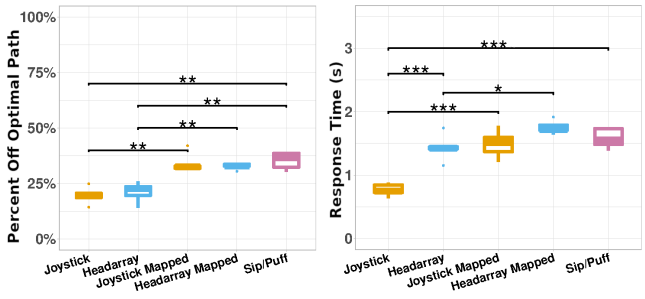

(a) (b)

Fig. 1: (a) Trajectory following performance. (b) Response time to prompted command. The notation $*$ implies a p-value of $p < 0.05$, $**$ implies $p < 0.01$, and $***$ implies $p < 0.001$.

We investigate the extent to which the physical activation mechanism and the mapping paradigm of an interface explain differences in usage characteristics. To that end, we perform a pilot study using three common interfaces employed by powered wheelchair users—namely, a joystick, headarray, and sip-n-puff (SNP). We evaluate the operation of these interfaces on two open-source computer game tasks designed to assess trajectory and command following performance [5], [20]. To understand the effect of how the signal is altered through the interface, in addition to the most common mappings, we also remap the joystick and headarray to match the constraints of the SNP interface. This is the only direction of remapping possible because the joystick and headarray are higher dimensional than the SNP. The results indicate that even though the physical mechanism of providing input is different, when the control mappings are similar, the usage characteristics are normalized across the interfaces (Figure 1). Moreover, under the constrained mappings the performance characteristics under joystick and headarray interfaces suffer, which motivates the need for an interface-aware assistance system that will compensate for the degradation in overall human-robot team performance.

Our approach to interface-aware signal interpretation is to explicitly model both how the physical actions are mapped to the task-level actions through the interface and how the user signal is stochastically altered through the interface.

IV. MATHEMATICAL FORMALISM

In this section we describe our mathematical model of the user's physical interaction with a control interface during manual teleoperation, and the assistive algorithm which uses our model to provide customized assistance.

A. Modeling the User's Physical Interface Operation

Figure 2 depicts the generative probabilistic graphical model of a user's physical interaction with a control interface during robot teleoperation at a single time step t.

Let w^t represent the true world state, o^t the partial observation of the world state, and $s_h^t \in \mathcal{S}$ the human's internal state that encodes the human's goals and beliefs. Let a^t denotes the action primitives that are defined in the task space (e.g., 'move forward', 'move backward', *et cetera*) that the user

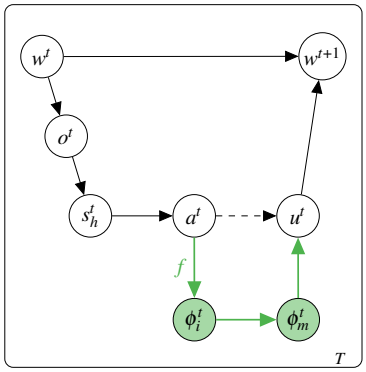

Fig. 2: Probabilistic graphical model depicting user-robot interaction via a control interface. Teleoperation is typically modeled simply as $a^t \rightarrow u^t$ (dashed edge). We additionally capture physical interaction with the interface (green nodes).

intends to execute and $\phi_i^t \in \Phi$ denote the ***intended*** *interface-level physical action* initiated by the user, that aims to achieve a^t and is *unobserved*. The set of available interface-level physical actions depends on the physical modality used for activating an interface. For example, SNP interface actions ϕ_i^t include 'Hard Sip' and 'Soft Puff'. The ***measured*** *interface-level physical action*, $\phi_m^t \in \Phi$, is fully *observed*. The low-level control commands issued to the robot is denoted as u^t. The mapping between ϕ_m^t and u^t is typically fixed.

The novel contribution of this model is in (a) the explicit modeling of the interface-dependent physical mechanisms that generate u^t and (b) in distinguishing the latent ϕ_i^t from the measured ϕ_m^t. In a noise-free setting, ϕ_i^t and ϕ_m^t are equivalent. However, in practice, ϕ_m^t may deviate from ϕ_i^t due to biases resulting from motor-impairment, stress, or equipment malfunction, to name a few. Modeling this distinction is important because the user desires ϕ_i^t to cause the transition in the world state, whereas in reality ϕ_m^t causes the transition, potentially into undesirable world states. An additional potential confound is faulty memory retrieval of the user's learned understanding of the inverse controller f that maps $a^t \rightarrow \phi_i^t$, which might occur due to time pressure, mental fatigue, or attention deficit [21], [22].

B. Estimation of a^t from Measured ϕ_m^t

We are interested in the following question: given the measured interface-level physical action issued by the user ϕ_m^t and the task context, what is the probability distribution over the task-level action primitives a^t? More precisely, we are interested in the probability distribution $p(a^t|\phi_m^t)$. Concretely, using Bayes theorem, we have

$$p(a^t|\phi_m^t) \propto p(\phi_m^t|a^t)p(a^t) \tag{1}$$

and marginalizing over ϕ_i^t results in,

$$p(\phi_m^t|a^t) = \Sigma_{\phi_i^t \in \Phi} p(\phi_m^t, \phi_i^t|a^t). \tag{2}$$

Due to the conditional independence of a^t and ϕ_m^t Equation 2 becomes

$$p(\phi_m^t|a^t) = \Sigma_{\phi_i^t \in \Phi} p(\phi_m^t|\phi_i^t)p(\phi_i^t|a^t) \tag{3}$$

and plugging Equation 3 into Equation 1 we have,

$$p(a^t|\phi_m^t) = \eta\, p(a^t)\Sigma_{\phi_i^t \in \Phi} p(\phi_m^t|\phi_i^t)p(\phi_i^t|a^t) \tag{4}$$

where η is the normalization factor. We also have

$$p(a^t) = \Sigma_{s_h^t \in \mathscr{S}} p(a^t|s_h^t)p(s_h^t) \tag{5}$$

and combining Equation 5 with Equation 4 gives us

$$p(a^t|\phi_m^t) = \eta \Sigma_{s_h^t \in \mathscr{S}} p(a^t|s_h^t)p(s_h^t) \left[\Sigma_{\phi_i^t \in \Phi} p(\phi_m^t|\phi_i^t)p(\phi_i^t|a^t) \right]. \tag{6}$$

Each one of the three conditional probability distributions that appear in the right hand side of Equation 6 have intuitive interpretations. $p(a^t|s_h^t)$ is the *control policy* the user follows during task execution. With training, practice, and learning, the user's policy will typically converge to an optimum—with respect to an internal cost function [23], [24], [25]. $p(\phi_i^t|a^t)$ captures the user's *internal model* of the true mapping (denoted as f) from task-level action primitives to the intended interface-level physical actions. Users acquire this internal model of f via training [26]. Finally, $p(\phi_m^t|\phi_i^t)$ captures the stochastic deviations of the *measured* interface-level physical actions from the *intended* interface-level physical actions and is the *user input distortion model*. These conditional probability distributions are user-specific can be learned from user teleoperation data.

C. Customized Handling of Unintended Physical Actions

The motivation for our framework described in Section IV-B is to improve the control of complex robotic machines with limited interfaces used by people with motor-impairments. Equation 6 can be used within a shared-control assistive paradigm to infer the human's true task-level intent and, if necessary, provide adjustments to reduce the cognitive and physical burden of unintentional deviations during interface operation. The inference scheme is outlined in Algorithm 1. Using Equation 6, at every time step t we compute the likelihood of $a^t \in \mathscr{A}$ conditioned on the observed ϕ_m^t (line 2). The action primitive corresponding to the maximum of the distribution is inferred to be the intended action $a_{inferred}^t$, and using the true control mapping function f we compute $\phi_{inferred}^t$ (lines 3-4). In Algorithm 2, the autonomy intervenes only if (a) $\phi_{inferred}^t$ is different from ϕ_m^t and (b) the uncertainty of prediction, computed as the entropy H of the distribution, is less than a predefined threshold ε. Otherwise, ϕ_m^t will be passed through the pipeline unaltered. The appealing characteristic of our proposed control-sharing algorithm is that the user is maximally in control, which potentially can improve user satisfaction and acceptance [27]. This is important for reasons of user adoption and cost. Furthermore, when the autonomy steps in, it does so only to provide commands closest to the user's true intentions (which they were unable to issue correctly themselves).

We implement and evaluate two assistive shared-control paradigms.

1) Filtered autonomy: If ϕ_m^t is deemed as unintended with certainty, filter (block) this command, $\phi_{corrected}^t = 0$, i.e., no motion or mode-switching occurs.

Algorithm 1 Infer Intended Commands

function INFER_INTENDED_COMMAND(t, ϕ_m^t)
  infer_intended_command
  compute $p(a^t|\phi_m^t)$ ▷ equation 6
  $a^t_{inferred} \leftarrow argmax((p(a^t|\phi_m^t))$
  $\phi^t_{inferred} \leftarrow f(a^t_{inferred})$ ▷ true control mapping
  return $\phi^t_{inferred}$

Algorithm 2 Handle Unintended Commands

function HANDLE_UNINTENDED_COMMANDS(t, ϕ_m^t)
  $\phi^t_{inferred}$ = INFER_INTENDED_COMMAND(t, ϕ_m^t)
  if $\phi^t_{inferred} \neq \phi^t_m$ **then**
    if $H(p(a^t|\phi_m^t)) < \varepsilon$ **then** ▷ uncertainty is low
      if filtered **then**
        $\phi^t_{corrected} = 0$
      else if corrective **then**
        $\phi^t_{corrected} = \phi^t_{inferred}$
    else
      return ϕ^t_m
  else
    return ϕ^t_m
  return $\phi^t_{corrected}$

2) Corrective autonomy: If ϕ^t_m is deemed as unintended with certainty, correct this command, $\phi^t_{corrected} = \phi^t_{inferred}$, i.e., resulting in the inferred intended action.

V. SIMULATION-BASED ALGORITHM EVALUATION

In order to gain a deeper insight into how different hyper-parameters—such as noise levels in $p(\phi_i^t|a^t)$ and $p(\phi_m^t|\phi_i^t)$—affect the performance of our assistance paradigm, we design a simulation-based experiment. We choose a path-navigation task for this evaluation and assume that an SNP interface is being used for robot teleoperation. The domain of task-level and interface-level actions for an SNP are defined in Section VI-A. Task-level action primitives (a^t) and intended interface-level physical actions (ϕ_i^t) are sampled from the generative model shown in Figure 2. ϕ_i^t is corrupted according to $p(\phi_m^t|\phi_i^t)$ to generate ϕ_m^t.

In our simulations, the distributions $p(\phi_i^t|a^t)$ and $p(\phi_m^t|\phi_i^t)$ are modeled as mixture distributions comprised of a delta and a uniform distribution. The weight factor ($w_{uniform}$) used for the mixture distributions is treated as a scalar simulation parameter.[1] The choice of mixture distributions for the simulation experiments helps to reveal the operation domain of the algorithm (rather than precisely corresponding to real-world distributions of $p(\phi_i^t|a^t)$ and $p(\phi_m^t|\phi_i^t)$). Table I indicates the ranges of all simulation parameters.

We evaluate the performance of our assistance algorithm as measured by the total number of state transitions during a trial, under different assistance conditions. Figure 3 reveals that a more accurate internal model (where $p(\phi_i^t|a^t)$ has low corruption noise), in general, will help the user to perform better. For a given $p(\phi_i^t|a^t)$, the corrective assistance paradigm has the highest performance, followed by filtered and no-assistance. The difference in performance between the assistance paradigms decreases as the noise in $p(\phi_i^t|a^t)$ increases, illustrating the need for proper training and acquisition of accurate internal models. These insights guide our experimental design explained in detail in the next section.[2]

[1] $w_{uniform} = 0.0$ and $w_{uniform} = 1.0$ denote a pure delta and uniform random distribution, respectively.

Parameter	Range of Values
N - Number of Turns	[1,2,3]
Assistance Type	[Filtered, Corrective, No Assistance]
$w_{uniform}$ in $p(\phi_i\|a)$	[0.1, 0.3, 0.5, 0.7]
$w_{uniform}$ in $p(\phi_m\|\phi_i)$	[0.1, 0.3, 0.5, 0.7]

TABLE I: Ranges of different simulation parameters.

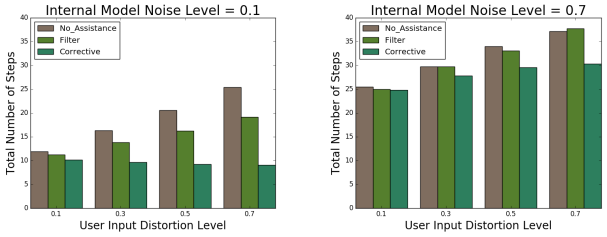

(a) (b)

Fig. 3: Total number of state transitions for two different noise levels in $p(\phi_i|a)$ - 0.1 (left) 0.7 (right).

VI. EXPERIMENTAL DESIGN

We ran a human-subject study ($n = 10$) to evaluate our inference algorithm and assistance paradigms in terms of overall task performance and user preference. All participants gave their informed, signed consent to participate in the experiment which was approved by Northwestern University's Institutional Review Board. Each study session consisted of three phases. Phase 1: Training and data collection to model $p(\phi_i^t|a^t)$, Phase 2: Training and data collection to model $p(\phi_m^t|\phi_i^t)$, and Phase 3: Assistance evaluation phase in which the subjects controlled a 3D point robot using the SNP interface under three distinct assistance conditions.

A. Experimental Testbed

For the evaluation task, we designed a simulated navigation environment with three control dimensions (Figure 4) [28]. Participants operated a 1D SNP interface, for reasons of difficulty and accessibility—this often is the only device accessible to those with severe motor impairments. The subjects used the SNP to operate a 3D point robot's motion along x, y or θ dimension, one at a time.[3] The set $\mathscr{A}$ of task-level action primitives consisted of (a) clockwise mode switch, (b) counter-clockwise mode switch, (c) positive direction motion, and (d) negative direction motion. The set

[2] Additional simulation results are included in the supplementary video.

[3] The dimensionality mismatch between the interface and the robot necessitates the control space to be partitioned into smaller subsets called *modes*. Motion is restricted only along those dimensions that belong to the currently active mode. The user can use the interface to activate different modes by switching between them, and this is referred to as *mode switching*.

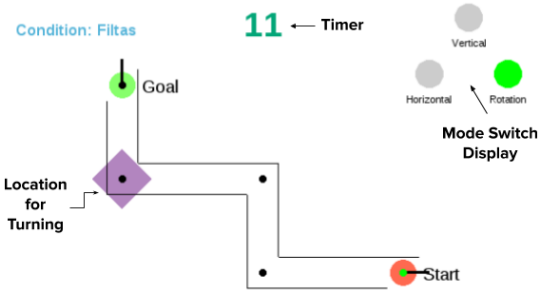

Fig. 4: An example trial in the human-subject study navigation environment. Feedback regarding the current active mode was displayed on the screen (on the top right corner).

Φ of interface-level physical actions available for a sip-and-puff were (a) hard sip, (b) soft sip, (c) hard puff, and (d) soft puff. The true correspondence between a^t and ϕ_i^t was deterministic (denoted as $f(\cdot)$) and predefined.

B. Learning Personalized Distributions

We designed two tasks to capture the personalized distributions $p(\phi_i^t|a^t)$ and $p(\phi_m^t|\phi_i^t)$ from user data.

1) Personalized Internal Control Mapping Model: Participants were first trained on the true mapping ($f(\cdot)$) during a standardized training phase. The training consisted of three phases: (a) learning about the action primitives (a^t) for the 3D experimental task-space (Figure 4), (b) learning about the interface-level physical actions (ϕ^t) available through the interface, and (c) the mapping between ϕ^t and a^t. The training was followed by six blocks of testing trials. During testing, the user was shown a graphical depiction of a^t, and instructed to select the correct ϕ^t. Each testing trial had a time limit of five seconds. The subjects repeated the training and the testing protocol until they met a minimum level of proficiency. The distribution $p(\phi_i^t|a^t)$ was modeled using data collected during the testing phase.

2) Personalized User Input Distortion Model: Participants were trained on the operation of the interface in order to ensure a good understanding of physical aspects of using the interface. During training, participants were asked to issue different interface-level actions and were provided feedback on how they performed. During testing, the user was shown an interface-level action on the screen (e.g., "Soft Puff") as a prompt and asked to generate the same action through the interface, with no feedback on performance. Each trial had a time limit of five seconds. The distribution $p(\phi_m^t|\phi_i^t)$ was modeled using the data collected during this testing phase.

C. Assistance Evaluation

In the evaluation task, the subject controlled the motion of a 3 Degrees-of-Freedom (DoF) point robot along predefined paths from a start pose to a goal pose. For each trial, the start and end positions were randomized. The initial control mode was selected at random, and restricted to be different than the mode corresponding to the optimal first action in order to normalize the difficulty of starting the trial in different configurations and ensure balance across action types. Users performed the evaluation task under three conditions: (1) *no assistance*, (2) *filtered* assistance, and (3) *corrective* assistance. The subject was required to rotate the point robot to the target orientation at one of the corners (highlighted in violet). Subjects were prompted to complete the task with the least number of mode switches and in a timely manner. A trial was deemed successful if the robot was at the goal pose within the allotted time limit (50 seconds). Subjects performed six blocks (two blocks per assistance condition) of six trials each. In total, we collected 360 trials (120 trials per assistance condition). After each block, the subjects were required to respond to a NASA-TLX questionnaire. At the end of the final block, the subjects filled out a post-session survey in which they rank-ordered the different assistance conditions according to their preference, intuitiveness, helpfulness, and difficulty.

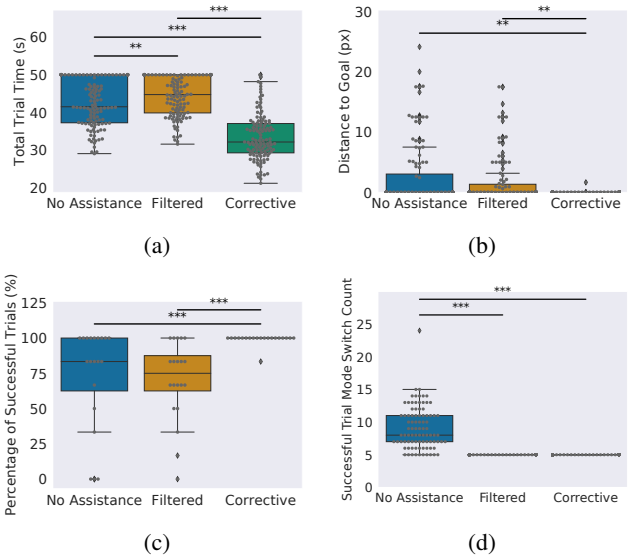

Fig. 5: Objective task performance metrics grouped by assistance condition. (a) Total trial time with maximum trial time capped at 50s. (b) Distance to the goal at the end of trials. (c) Percentage of successful trials. (d) Total number of mode switches during successful trials. All metrics improve significantly with the corrective assistance condition.

VII. RESULTS

We analyze group performances using the non-parametric Kruskal-Wallis test and perform the Conover's test post-hoc pairwise comparisons to find the strength of significance.[4]

A. Objective Task Performance Metrics

To evaluate the effectiveness of our algorithm on overall task performance, we compare (1) the total task completion times, (2) the distance to the desired goal position and orientation at the end of each trial, (3) the percentage of successful trials under each assistance condition, and (4) the total number of mode switches for successful trials, across the three assistance conditions (Figure 5).

[4]For all figures, $*: p < 0.05$, $**: p < 0.01$, and $***: p < 0.001$.

As seen in Figure 5a, the total trial time is shortest under *corrective* assistance, increases with the *no assistance*, and is largest under the *filtered* assistance paradigm. One likely reason for the latter observation is that under *filtered* assistance, the repeated issuance of suboptimal mode switch commands is repeatedly blocked, while under *no assistance* consecutive suboptimal mode switches are executed and potentially end in the desired control mode. For example, in our experimental setup, two counter-clockwise mode switches is equivalent to a single clockwise mode switch, and vice versa.

Figures 5b-5c show the distance to goal at the end of the trial and the percentage of trials successfully finished by each subject, respectively. Both of these metrics improve significantly under the *corrective* assistance condition.

The *filtered* and *corrective* assistance paradigms are comparable when looking at the total number of mode switches during successful trials (Figure 5d). Both assistance conditions are optimal with respect to the number of mode switches, which is five for all trials. Under *no* assistance, despite successful task completion, the number of executed mode switches is up to three times the optimal number.

B. Subjective Task Performance Metric

We use the raw NASA-TLX as a subjective measure of perceived workload [29]. Larger TLX scores indicate higher perceived workloads. During corrective assistance, the autonomy offloads some of the cognitive burden by correcting unintended actions—as evident by the significant reduction in the user's perceived workload (Figure 6). During filtered assistance, although the autonomy gives feedback by way of blocking unintended actions, the user is still responsible for issuing all correct commands.

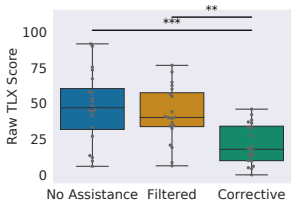

Fig. 6: Perceived workload measured by the NASA-TLX score, grouped by assistance condition.

C. User Acceptance of Assistive Autonomy

We evaluate user preferences and acceptance of our shared-control assistive paradigms using a questionnaire (Figure 7). The statements are rated on a 7-point Likert scale from strongly disagree (1) to strongly agree (7). Although some of the objective measures of task performance between *filtered* assistance and *no assistance* are comparable, the users rate that the *filtered* assistance helps them complete the task more efficiently and is easier to operate than under *no assistance*. Overall, the participants show a strong preference for the *corrective* assistance.

VIII. DISCUSSION AND IMPLICATIONS

Our results suggest that each of the assistance paradigms have unique advantages that are crucial for end users of assistive devices. In particular, since the *filtered* paradigm blocks all user inputs that do not correspond to optimal

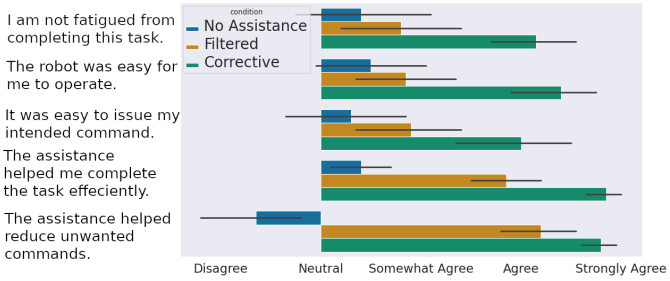

Fig. 7: Average user response to post-task questionnaire. The bars indicate standard deviation.

actions, a user operating the interface under this condition can learn to issue the correct commands. This paradigm can potentially be used within a rehabilitative setting with various methods of feedback as a teleoperation training paradigm to assist in maximal skill acquisition. By contrast, the *corrective* paradigm might help users who have plateaued in their skill in operating the interface, or in cases where efficient and successful task completion is critical. A person with a recent motor impairment could begin to operate an assistive device earlier in their rehabilitation journey with corrective assistance, thereby accelerating their mobility independence. When used in tandem within a shared-control framework, the proposed assistance paradigms have the potential to improve the quality of device operation while also encouraging skill development, and making independent operation of the device more accessible.

In our future work, we intend to explicitly model fatigue and learning dynamics, and study their impact on each of the personalized distributions. We also will explore various synergies that arise as a result of the human operator's co-adaptation to the robotic autonomy.

IX. CONCLUSIONS

We have presented a probabilistic graphical model of user-robot interaction that distinguishes between intended versus measured user control signals. We introduced two assistance paradigms that reason about stochastic deviations in user input in a shared-control framework. The efficacy of the assistance paradigms were evaluated both in simulation and via a human subject study. Our results demonstrated improvements in objective task metrics as well as user perception metrics.

ACKNOWLEDGMENT

This material is based upon work supported by the National Science Foundation under Grants IIS-1552706 and CNS-1544741, and U.S. Office of Naval Research under the Award Number N00014-16-1-2247. Any opinions, findings, and conclusions or recommendations expressed in this material are those of the authors and do not necessarily reflect the views of the National Science Foundation or the U.S. Office of Naval Research.

REFERENCES

[1] Chih-Hung King, Tiffany L Chen, Zhengqin Fan, Jonathan D Glass, and Charles C Kemp. Dusty: an assistive mobile manipulator that retrieves dropped objects for people with motor impairments. *Disability and Rehabilitation: Assistive Technology*, 7(2):168–179, 2012.

[2] Sven Cremer, Fahad Mirza, Yathartha Tuladhar, Rommel Alonzo, Anthony Hingeley, and Dan O Popa. Investigation of human-robot interface performance in household environments. In *Sensors for Next-Generation Robotics III*, volume 9859, page 985904, 2016.

[3] Jing Luo, Zhidong Lin, Yanan Li, and Chenguang Yang. A teleoperation framework for mobile robots based on shared control. *IEEE Robotics and Automation Letters*, 5(2):377–384, 2019.

[4] Brice Rebsamen, Cuntai Guan, Haihong Zhang, Chuanchu Wang, Cheeleong Teo, Marcelo H Ang, and Etienne Burdet. A brain controlled wheelchair to navigate in familiar environments. *IEEE Transactions on Neural Systems and Rehabilitation Engineering*, 18(6):590–598, 2010.

[5] Mahdieh Nejati Javaremi, Michael Young, and Brenna D Argall. Interface operation and implications for shared-control assistive robots. In *Proceedings of the International Conference on Rehabilitation Robotics (ICORR)*, 2019.

[6] Mark M Churchland, Afsheen Afshar, and Krishna V Shenoy. A central source of movement variability. *Neuron*, 52(6):1085–1096, 2006.

[7] A Aldo Faisal, Luc PJ Selen, and Daniel M Wolpert. Noise in the nervous system. *Nature Reviews Neuroscience*, 9(4):292–303, 2008.

[8] Robert J Van Beers, Patrick Haggard, and Daniel M Wolpert. The role of execution noise in movement variability. *Journal of Neurophysiology*, 91(2):1050–1063, 2004.

[9] Icek Ajzen, Thomas C Brown, and Franklin Carvajal. Explaining the discrepancy between intentions and actions: The case of hypothetical bias in contingent valuation. *Personality and Social Psychology Bulletin*, 30(9):1108–1121, 2004.

[10] Marc W Slutzky and Robert D Flint. Physiological properties of brain-machine interface input signals. *Journal of Neurophysiology*, 118(2):1329–1343, 2017.

[11] Firas Abi-Farrajl, Bernd Henze, Alexander Werner, Michael Panzirsch, Christian Ott, and Máximo A Roa. Humanoid teleoperation using task-relevant haptic feedback. In *Proceedings of the IEEE/RSJ International Conference on Intelligent Robots and Systems (IROS)*, 2018.

[12] Camilla Pierella, A Sciacchitano, Ali Farshchiansadegh, Maura Casadio, and SA Mussa-Ivaldi. Linear vs non-linear mapping in a body machine interface based on electromyographic signals. In *Proceedings of the IEEE International Conference on Biomedical Robotics and Biomechatronics (Biorob)*, pages 162–166, 2018.

[13] Alex Pentland and Andrew Liu. Modeling and prediction of human behavior. *Neural Computation*, 11(1):229–242, 1999.

[14] Michael Bowman, Songpo Li, and Xiaoli Zhang. Intent-uncertainty-aware grasp planning for robust robot assistance in telemanipulation. In *Proceedings of the IEEE International Conference on Robotics and Automation (ICRA)*, 2019.

[15] Siddharth Reddy, Anca Dragan, and Sergey Levine. Where do you think you're going?: Inferring beliefs about dynamics from behavior. In *Proceedings of the Neural Information Processing Systems (NeurIPS)*, 2018.

[16] Anna N Rafferty, Michelle M LaMar, and Thomas L Griffiths. Inferring learners' knowledge from their actions. *Cognitive Science*, 39(3):584–618, 2015.

[17] Dylan P Losey, Craig G McDonald, Edoardo Battaglia, and Marcia K O'Malley. A review of intent detection, arbitration, and communication aspects of shared control for physical human–robot interaction. *Applied Mechanics Reviews*, 70(1), 2018.

[18] Henny Admoni and Siddhartha Srinivasa. Predicting user intent through eye gaze for shared autonomy. In *Proceedings of the AAAI Fall Symposium Series*, 2016.

[19] Shervin Javdani, Siddhartha S Srinivasa, and J Andrew Bagnell. Shared autonomy via hindsight optimization. In *Proceedings of the Robotics Science and Systems (RSS)*, 2015.

[20] M. Nejati Javaremi, M. Young, and B Argall. Chicago, IL, USA. interface assessments (v1.0). [Online]. Available: `https://github.com/argallab/interface_assessments`, 2019.

[22] Mathias Luethi, Beat Meier, and Carmen Sandi. Stress effects on working memory, explicit memory, and implicit memory for neutral and emotional stimuli in healthy men. *Frontiers in Behavioral Neuroscience*, 2:5, 2009.

[23] Masao Ito. Internal model visualized. *Nature*, 403(6766):153–154, 2000.

[24] Richard J Jagacinski and Richard A Miller. Describing the human operator's internal model of a dynamic system. *Human Factors*, 20(4):425–433, 1978.

[25] JoAnn Kluzik, Jorn Diedrichsen, Reza Shadmehr, and Amy J Bastian. Reach adaptation: what determines whether we learn an internal model of the tool or adapt the model of our arm? *Journal of Neurophysiology*, 100(3):1455–1464, 2008.

[26] Camilla Pierella, Maura Casadio, Ferdinando A Mussa-Ivaldi, and Sara A Solla. The dynamics of motor learning through the formation of internal models. *PLoS Computational Biology*, 15(12):e1007118, 2019.

[27] Alex Broad, Todd Murphey, and Brenna Argall. Highly parallelized data-driven MPC for minimal intervention shared control. *Proceedings of Robotics: Science and Systems (RSS)*, 2019.

[28] D. Gopinath, M. Nejati Javaremi, and B Argall. Chicago, IL, USA. customized interface-aware assistance (v1.0). [Online]. Available: `https://github.com/argallab/customized_interface_aware_assistance.git`, 2020.

[29] Sandra G Hart. NASA-task load index (NASA-TLX); 20 years later. In *Proceedings of the Human Factors and Ergonomics Society Annual Meeting*, 2006.